MULTICANONICAL MONTE CARLO STUDY AND ANALYSIS OF TAILS FOR THE ORDER-PARAMETER DISTRIBUTION OF THE TWO-DIMENSIONAL ISING MODEL

R. HILFER, B. BISWAL, H.G. MATTUTIS, AND W. JANKE

Abstract. The tails of the critical order-parameter distribution of the two-dimensional Ising model are investigated through extensive multicanonical Monte Carlo simulation. Results for fixed boundary conditions are reported here, and compared with known results for periodic boundary conditions. Clear numerical evidence for "fat" stretched exponential tails exists below the critical temperature, indicating the possible presence of fat tails at the critical temperature. Our work suggests that the true order parameter distribution at the critical temperature must be considered to be unknown at present.

Key words and phrases. PACS: 05.50.+q, 64.60.Cn, 64.60.Fr, 05.70.Ln.

[page 68, §1]

I. Introduction

[68.1.1.1] A quantity of central importance for finite-size scaling analysis of critical phenomena is the order parameter distribution [1, 2]. *[68.1.1.2]* Despite many years of research there remain open questions even for the much studied case of the Ising universality class [3, 4, 5, 6, 7, 8, 9, 10, 11, 12].

[68.1.2.1] Most properties of the critical order parameter distribution $p(m)$ are known from computer simulations [13, 14, 6, 11]. Analytical information comes from field theoretic renormalization group calculations [15, 16, 7], from conformal field theory [17] and also from a generalized classification theory of phase transitions [18, 19, 20, 21, 22, 23]. *[68.1.2.2]* In Refs. [23, 3] some of the analytical predictions seem to have been corroborated by numerical simulations. *[68.1.2.3]* On the other hand the simulations in Refs. [23, 3] were not able to corroborate the predictions for the tails of the critical order parameter distribution. *[68.1.2.4]* Recording of the very small probabilities in the tails requires special techniques such as multicanonical simulations. *[68.1.2.5]* Even in a multicanonical simulation it is necessary to accumulate sufficient statistics in order to probe the tails and to be able to distinguish different theoretical predictions. *[68.1.2.6]* Many different simulations [3, 4, 9, 10] in recent times have attempted this, but failed in establishing the true behavior at the tails of the critical order parameter distribution.

[68.1.3.1] Detailed investigations of the tails were carried out in one of the early multi-canonical Monte Carlo simulation [4] for the critical two dimensional Ising model (square lattice of size $L = 32$ and $L = 64$). *[68.1.3.2]* Even though this work measured extremely small tail probabilities with remarkably high precision, no power law behavior was observed for large magnetization. *[68.1.3.3]* In addition this simulation could not establish convincingly the agreement of the finite-size scaling predictions in the far tail regime.

[68.1.4.1] Given the observations of non-Gaussian "fat tails" in many other physical phenomena, and following the predictions of the generalized classification theory [23, 3], a recent work [9] has tried to ascertain the behavior in the tails of critical order-parameter distribution through high precision Monte Carlo simulation (Swendsen-Wang cluster flip algorithms) of square and simple cubic Ising models at $T = T_c$ with a mixture of free and helical boundary conditions. *[68.2.0.2]* The work concludes that in two and three dimensions the tails of the distribution are consistent with Gaussian behaviour even at the critical point.

[68.2.1.1] A more recent high-precision Monte Carlo study [10] of the probability distribution of the order parameter for the three-dimensional Ising model ($L = 12$ to 58) at $T = T_c$ presents a phenomenological formula (different from a plain Gaussian distribution) that describes well the main peak of the measured distribution but excludes the far tail regime. *[68.2.1.2]* This simulation based on Swendsen-Wang cluster flip algorithms with periodic boundary condition also reports some discrepancy with earlier estimates [9].

[68.2.2.1] In the present paper we report results of high precision multicanonical Monte Carlo (MCMC) simulation for the Ising model on square lattices with periodic and fixed (i.e. all boundary spins fixed to +1) boundary conditions. *[68.2.2.2]* Our central objective is to study whether the order parameter distribution obtained from the simulation can be considered to be asymptotic with respect to the number of Monte-Carlo steps (MCS-convergence) and system size (L-convergence). *[68.2.2.3]* A secondary objective is to study fixed (symmetry breaking) boundary conditions because the asymmetry of the order parameter distribution should give rise to an asymmetry in the far tail behaviour. *[68.2.2.4]* Different boundary conditions are important for the study of critical finite-size scaling functions. *[68.2.2.5]* We study the two-dimensional Ising model, firstly because exact analytical results are available, and secondly because we expect the true tail behaviour to emerge more quickly in this case.

[68.2.3.1] The paper is organized in the following manner. *[page 69, §0]* *[69.1.0.1]* In Section II we recall the basic quantities and assumptions from finite-size scaling. *[69.1.0.2]* In Section III the MCMC simulation method is described and convergence with respect to system size and number of Monte Carlo steps is discussed briefly. *[69.1.0.3]* The data analysis, results, and the discussion are presented in Section IV.

II. Critical finite-size scaling functions

[69.1.1.1] We consider the two-dimensional Ising model on a square lattice of side length L. *[69.1.1.2]* The $N = L^2$ spins $\sigma_i = \pm 1$ interact according to the Hamiltonian $\mathcal{H} = -J \sum_{(i,j)} \sigma_i \sigma_j - H \sum_{i=1}^{N} \sigma_i$ where $J > 0$ is the ferromagnetic coupling strength and H is an external field. *[69.1.1.3]* The first summation $\sum_{(i,j)}$ runs over all nearest neighbour pairs on the lattice. *[69.1.1.4]* The order parameter is the magnetization per spin

$$m = \frac{1}{N} \sum_{i=1}^{N} \sigma_i \tag{1}$$

whose value fulfills $-1 \le m \le 1$. *[69.1.1.5]* In the following we set $J = 1$ and also the Boltzmann constant to unity. *[69.1.1.6]* We denote the temperature by T, and write $h = H/(k_B T)$ for the magnetic field.

[69.1.2.1] In this paper we focus on the probability density $p(m)$ of the order parameter defined as

$$p(m) = \frac{\sum_{\{\sigma\}} \delta\left(\sum_{i=1}^{N} \sigma_i, Nm\right) \exp(-\beta\mathcal{H})}{\sum_{\{\sigma\}} \exp(-\beta\mathcal{H})} \tag{2}$$

where $\beta = 1/(k_B T)$, $\delta(i,j) = \delta_{ij}$ is a Kronecker δ, and where m is such that $|Nm/2|$ is an integer not larger than $N/2$. *[69.1.2.2]* The probability density $p(m)$ depends parametrically on temperature T, field h and system size $N = L^2$,

$$p(m) = p(m; T, h, L). \tag{3}$$

[69.1.2.3] It is also called order parameter distribution. *[69.1.2.4]* In the following we limit ourselves to the case $h = 0$, and hence $p(m) = p(m; T, L)$. *[69.1.2.5]* The critical order parameter distribution is obtained in the limit $L \to \infty$ and $T \to T_c$ where $T_c = 2/\mathrm{arsinh}(1) \approx 2.2691853...$ is the critical temperature. *[69.1.2.6]* There are different ways of taking this limit (see [23] for an overview). *[69.1.2.7]* Traditionally this limit is understood as the finite-size scaling limit defined by

$$L \to \infty,\ T \to T_c \qquad \text{such that} \qquad L/\xi \approx 1 < \infty \tag{4}$$

where $\xi = \xi(T)$ is the temperature dependent spin-spin-correlation length for the infinite system. *[69.1.2.8]* Note that in an infinite system $\xi(T) \to \infty$ as $T \to T_c$. *[69.1.2.9]* A second way to take the limit is the finite ensemble scaling limit defined through [23]

$$L \to \infty,\ T \to T_c \qquad \text{such that} \qquad L/\xi \to \infty. \tag{5}$$

[69.2.0.10] All other possibilities for taking the limits are discussed in [23]. *[69.2.0.11]* It is often postulated that ξ fulfills the finite size scaling hypothesis

$$\xi(t, L) = L\widetilde{\xi}(tL^{1/\nu}) \tag{6}$$

in the finite-size scaling limit. *[69.2.0.12]* Here $t = (T - T_c)/T_c$ is the reduced temperature, $\widetilde{\xi}(x)$ is a universal scaling function and ν is the correlation length exponent. *[69.2.0.13]* For the two-dimensional Ising model $\nu = 1$.

[69.2.1.1] The traditional finite-size scaling hypothesis [13, 24] for the critical order parameter distribution assumes that

$$p(m; T = T_c, L) = p(m; L) = L^{\beta/\nu}\widetilde{p}(mL^{\beta/\nu}) \tag{7}$$

where $\widetilde{p}(x)$ is the universal scaling function of the order parameter distribution and β is the order parameter exponent. *[69.2.1.2]* For the two-dimensional Ising model [25]

$$\beta = \frac{1}{8}. \tag{8}$$

[69.2.1.3] Our scaling variable is then

$$x = mL^{1/8}. \tag{9}$$

[69.2.1.4] Using the scaling assumption (7) one obtains the absolute moments of the critical order parameter distribution

$$\langle |m|^k \rangle(L) = \int |m|^k p(m; L)\mathrm{d}m = L^{-k\beta/\nu}\widetilde{m}_k \tag{10}$$

where

$$\widetilde{m}_k = \int |x|^k \widetilde{p}(x)\mathrm{d}x. \tag{11}$$

[69.2.1.5] From these one calculates the so called renormalized coupling constant $g = \widetilde{m}_4/\widetilde{m}_2^2$ or the Binder cumulant

$$U_L = 1 - \frac{\widetilde{m}_4}{3\widetilde{m}_2^2} \tag{12}$$

which are often used in studies of critical behaviour because they are independent of L at criticality, if all the assumptions are valid.

III. Simulation Methods and Boundary Conditions

A. Multicanonical Monte-Carlo (MCMC) Simulation

[69.2.2.1] Monte Carlo (MC) simulations with simple sampling (SS) probe configurations according to their geometrical multiplicity and re-weight them with their thermodynamic probability $\exp(-\beta E_i)$, so for an observable A the average is computed as

$$\langle A \rangle_{SS} = \frac{\sum_i A_i \exp(-\beta E_i)}{\sum_i \exp(-\beta E_i)}. \tag{13}$$

[page 70, §0] *[70.1.0.1]* Standard importance sampling (IS) methods like the Metropolis-algorithm accept and reject configurations according to their relative thermodynamic probability, so that the thermodynamic weight is built into the sampling process instead of the re-weighting, and therefore the thermodynamic average reduces to a simple average

$$\langle A \rangle_{IS} = \frac{\sum_i A_i}{\sum_i 1}. \tag{14}$$

[70.1.0.2] In some cases, Metropolis-type sampling can be inefficient because some configurations may be "rare" with respect to their thermodynamic weight, but "important" because their contribution A_i is disproportionately large, or because the range with small probability contains a "barrier" to cross so that other, more "important" configurations can be reached. *[70.1.0.3]* To overcome this problem of sampling "rare events", Berg and Neuhaus [26] proposed a method that modifies the importance sampling procedure in such a way that "artificial"

probabilities P_i are introduced for each A_i. *[70.1.0.4]* Because not a single canonical sampling is used, but each observable lives on it's "own" canonical average, the method was called "multi-canonical Monte Carlo" (MCMC). *[70.1.0.5]* The Metropolis-type averages of eq. (14) are then modified to

$$\langle A\rangle_{MCMC} = \frac{\sum_i A_i P_i}{\sum_i P_i}. \tag{15}$$

[70.1.0.6] The weights P_i can be chosen for convenience, e.g. in such a way that all A_i are sampled uniformly, or some part of the phase space is sampled with higher frequency than another part [27].

B. Implementation

[70.1.1.1] We implemented a Monte-Carlo algorithm on a square grid with Glauber dynamics. *[70.1.1.2]* The grid has an even number of sites in each direction, so that we can use the checker-board update scheme, which has the smallest correlation time [28] under all single-spin update-schemes in the straightforward Metropolis-algorithm. *[70.1.1.3]* Our Fortran 90 program using sub-arrays allowed a simple implementation of fixed or periodic boundaries. *[70.1.1.4]* We choose not to implement bit-coding, as the bulk of the computer time would be spent in updating the information of the MCMC-procedure rather than for the straightforward algorithm. *[70.1.1.5]* The implementation using non-overlapping sub-arrays also allows vectorization. *[70.1.1.6]* In addition we parallelized the algorithm.

[70.1.2.1] To sample the magnetizations evenly, the weights P_i in eq. (15) is chosen according to the magnetization, $P_i = P(M_i)$. *[70.1.2.2]* The MCMC proceeds in several iterations j, during which the intermediate $P_i^{(j)}$ are consecutively refined using the previously computed entries so that $P_i^{(j)} \to P_i$ are obtained. *[70.1.2.3]* Probabilities $P_i^{(j)}$ are evaluated from the histogram of the visited magnetizations during each spin update. *[70.1.2.4]* Details of our algorithm for the magnetization distribution will be published elsewhere.

C. Convergence

[70.2.1.1] The objective of our Monte-Carlo simulations is to obtain information about the equilibrium states (i.e. long time limit) for an infinite system (i.e. large L limit).

[70.2.2.1] We must distinguish between two kinds of convergence:

- MCS-convergence: By this we mean that, at given L and T, the individual simulation run is converged in the sense that increasing the number of Monte-Carlo steps (MCS) will not change the order parameter distribution. The measured distribution is the "true" distribution for the given system size and temperature.
- L-convergence: By this we mean the convergence of the distribution with L at given T to its form for the infinite system.

[70.2.3.1] The autocorrelation time needed by the algorithm to go from large negative magnetizations to large positive magnetizations increases rapidly as the system size becomes large.

[70.2.4.1] Therefore it is difficult to obtain fully MCS-converged results at large system sizes. *[70.2.4.2]* Because we are interested only in the tail behaviour we need to exclude all cutoffs not resulting from the system size, and hence need fully MCS-converged results.

[70.2.5.1] Within available resources and with simulation for 10^5 Monte Carlo steps per iteration and 50 multicanonical iterations on a Cray-T3E with 128 processors we could obtain statistics all the way up to the saturation magnetization for system sizes $L = 16,\ 32,\ 64$. *[70.2.5.2]* Simulations for $L = 128$ did not MCS-converge fully within the available computer time. *[70.2.5.3]* For $L = 128$ the simulation runs do not reach $m = 1$, and achieve statistics only upto $m = 0.95$. *[70.2.5.4]* Although this is a significant improvement over the tails statistics presented in Ref. [9], it is still not sufficient for our tail analysis. *[70.2.5.5]* Therefore our results below are limited to system sizes $L \leq 64$.

D. Far tail regime

[70.2.6.1] MCMC simulations of the two-dimensional Ising model provide far better statistics in the tails than the Swendsen-Wang cluster flip algorithm [9]. *[70.2.6.2]* As discussed in Section II adequate statistics is required in the "far tail regime" close and prior to saturated magnetization. *[70.2.6.3]* This regime is defined as

$$m_{\rm mp} \ll m \ll 1 \tag{16}$$

where m is the magnetization per spin and $m_{\rm mp}$ is the most probable magnetization. *[70.2.6.4]* We define the position of the (local or global) maxima of $p(m)$ as the most probable magnetization denoted by $m_{\rm mp}(T, L)$. *[70.2.6.5]* For the scaling variable defined in eq. (9) this implies

$$x_{\rm mp} \ll x \ll L^{1/8}. \tag{17}$$

[page 71, §1]

E. Boundary Conditions

[71.1.1.1] Most previous investigations have concentrated on periodic boundary conditions. *[71.1.1.2]* These boundary conditions have the advantage of preserving the fundamental symmetry. *[71.1.1.3]* In this paper we

present also results for fixed symmetry breaking boundary conditions where all boundary spins are fixed to +1.

[71.1.2.1] Our motivation for investigating fixed boundary conditions comes from Ref. [23]. In particular one expects that the order parameter distribution becomes asymmetric, and this raises the question whether or not the left and the right tail behave in the same way.

IV. Results

A. Results for moments and cumulants

[71.1.3.1] In Figure 1 we compare the Binder cumulant for periodic and fixed boundary conditions. *[71.1.3.2]* We notice that for fixed boundary conditions the values lie generally above those for the periodic case. *[71.1.3.3]* They are very close to their upper limit $U_L = 2/3$, that is expected for a nonvanishing first moment.

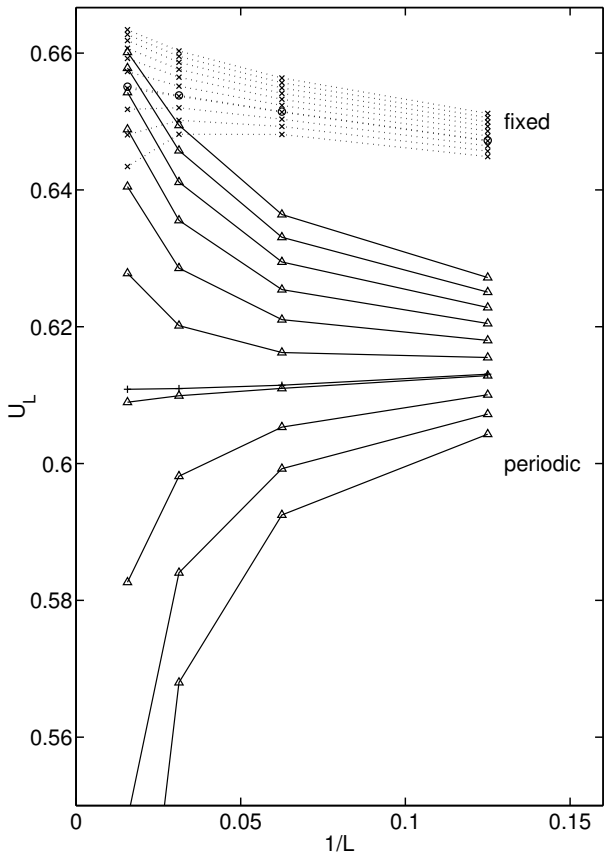

FIGURE 1. Cumulant U_L versus $1/L$ for fixed and periodic boundary conditions. Individual curves correspond to $T =$ 2.21, 2.22, 2.23, 2.24, 2.25, 2.26, 2.2691, 2.27, 2.28, 2.29, 2.3 from top (low T) to bottom (high T). The curves for T_c are marked with a special symbol (+ for periodic and ∘ for fixed boundary conditions).

B. Results for maxima

[71.1.4.1] For fixed boundary conditions the function $p(m; T, L)$ has a single maximum as a function of m for all values of T and L. *[71.1.4.2]* For periodic boundary conditions on the other hand there exists a temperature $T^*(L)$ above which the distribution has a single maximum, below which it has two local maxima. *[71.1.4.3]* For $L \to \infty$ the most probable magnetization approaches the exact infinite volume magnetization given by

$$m_{\rm ex}(T) = \begin{cases} \pm\left(1 - (\sinh(2/T))^{-4}\right)^{1/8} & \text{for } T < T_c \\ 0 & \text{for } T \geq T_c. \end{cases} \quad (18)$$

[71.1.4.4] Therefore we utilize the difference

$$\Delta(T, L) = m_{\rm mp}(T, L) - m_{\rm ex}(T) \quad (19)$$

as a measure for the convergence to the infinite volume result. *[71.1.4.5]* Here $m_{\rm mp}$ is the most probable magnetization defined earlier.

[71.1.5.1] In Figure 2 we plot this difference as a function of temperature for system sizes $L = 16, 32, 64$ for the case of fixed boundary conditions. *[71.1.5.2]* One sees that for $T \ll T_c$ the difference is small. *[71.1.5.3]* For $T \gg T_c$ the difference is rather large. *[71.1.5.4]* This is surprising, as we shall see in more detail below. *[71.1.5.5]* One also sees a pronounced maximum around T_c. *[71.1.5.6]* The height of the maximum is so large that the results are clearly not L-converged around T_c. *[71.1.5.7]* The asymptotic value for the maximum value at $T = T_c$ is $m = 0$ for all boundary conditions. *[71.2.0.8]* There is no reason to believe that the shape of the critical order parameter distribution has reached its asymptotic limit, if

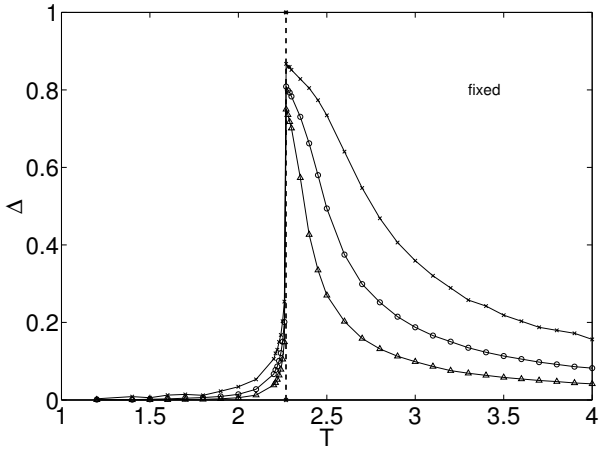

FIGURE 2. Difference $\Delta(T, L)$ defined in (19) between the most probable magnetization $m_{\rm mp}(T, L)$ and the exact infinite volume magnetization $m_{\rm ex}(T)$ versus temperature for fixed boundary conditions. Different curves correspond to system sizes $L = 16(\times)$, $L = 32(\circ)$ and $L = 64(\triangle)$. The vertical dashed line marks T_c.

its peak (maximum value) has not reached its asymptotic limit.

[71.2.1.1] In Figure 3 we plot $\Delta(T, L)$ for the case of periodic boundary conditions. *[71.2.1.2]* In this case there are two local maxima below T_c and in the critical region. *[71.2.1.3]* Hence there are two curves. *[71.2.1.4]* Compared to the case of fixed boundary conditions the deviations above T_c appear to be smaller. *[71.2.1.5]* A more detailed comparison to Gaussian behaviour, to be performed below, shows that the deviations above T_c are comparable to those in the fixed case.

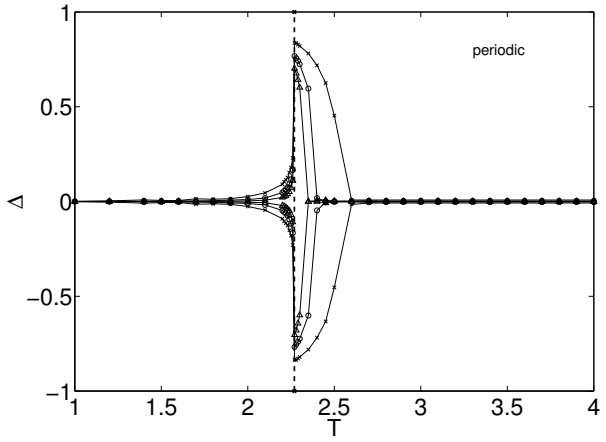

FIGURE 3. Difference $\Delta(T, L)$ defined in (19) between the most probable magnetization $m_{\rm mp}(T, L)$ and the exact infinite volume magnetization $m_{\rm ex}(T)$ versus temperature for periodic boundary conditions. Different curves correspond to system sizes $L = 16(\times)$, $L = 32(\circ)$ and $L = 64(\triangle)$. The vertical dashed line marks T_c.

C. **Results for tails**

[71.2.2.1] Here we analyze the tails of $p(m)$. *[71.2.2.2]* First we find numbers A, B such that the rescaled function

$$p_0(x) = Ap(B(m - C)) \tag{20}$$

where $x = B(m - C)$ and $p_0 = Ap$ has mean zero, unit norm and unit variance. *[71.2.2.3]* To facilitate the comparison between periodic and fixed boundary conditions the data for periodic boundary conditions were treated somewhat differently than it is normally done. *[71.2.2.4]* In the periodic case eq. (20) is applied not to $p(m)$ itself but only to its right half, i.e. the data for $m > 0$. *[71.2.2.5]* In Figure 4 we show the rescaled functions $p_0(x)$ at criticality $T = T_c$ for fixed and periodic boundary conditions. *[71.2.2.6]* The data collapse at T_c is found to be generally good.

[71.2.3.1] To analyze the tails we split the function $p_0(x)$ at the peak into the left and right tail. *[71.2.3.2]* More precisely we find the functions

$$\begin{aligned} p_{0r}(x) &= p_0(x - x_{\rm peak}) \qquad \text{for } x > x_{\rm peak} \\ p_{0l}(x) &= p_0(x_{\rm peak} - x) \qquad \text{for } x < x_{\rm peak} \end{aligned} \tag{21}$$

where $x_{\rm peak}$ is the position of the maximum. *[71.2.3.3]* To exhibit stretched exponential tails we calculate the functions

$$q(y) = \frac{\mathrm{d}\log_{10}(-\log_{10} p_{0i})}{\mathrm{d}\log_{10} x} \tag{22}$$

where $i = l, r$ and plot them against $y = \log_{10} x$. *[71.2.3.4]* In this way of plotting the data a tail of the form $p_0(x) \sim B(x + c)^\beta \exp(-A(x + c)^\alpha)$ corresponds to the function

$$q(y) = \alpha\left(1 - \frac{cf_A - f_B + (\beta 10^y)/(\alpha(10^y + c))}{(10^y + c)f_A - f_B}\right) \tag{23}$$

where $f_A = A(10^y + c)^{\alpha-1}$ and $f_B = \ln B + \beta \ln(10^y + c)$. *[71.2.3.5]* The exponent α can be easily identified as a plateau at the value α. *[71.2.3.6]* In these plots the far tail regime corresponds to large values of x. *[71.2.3.7]* A standard normal (Gaussian) distribution $(1/\sqrt{2\pi})\exp(-x^2/2)$ corresponds to the function

$$g(y) = 2\left(1 - \frac{\log_{10}(2\pi)}{\log_{10}(\mathrm{e})10^{2y} + \log_{10}(2\pi)}\right) \tag{24}$$

[page 72, §0] where $y = \log_{10} x$. *[72.1.0.1]* We note that our choice to split $p_0(x)$ at the peaks is natural, and we believe, the only reasonable choice away from T_c. *[72.1.0.2]* At T_c, multiplication of algebraic prefactors or splitting the distribution differently into right and left tails does not affect the results of the following analysis of the far tail region.

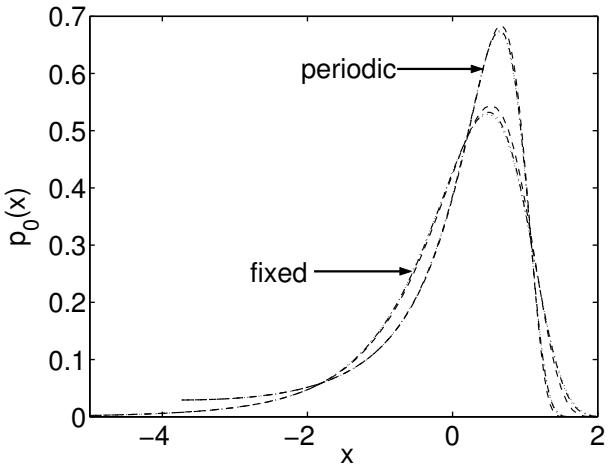

FIGURE 4. Rescaled order parameter distributions $p_0(x)$ for $T = T_c$ and $L = 16, 32, 64$ for fixed and periodic boundary conditions. (Only the right half of the distribution is scaled and shown for periodic boundary conditions).

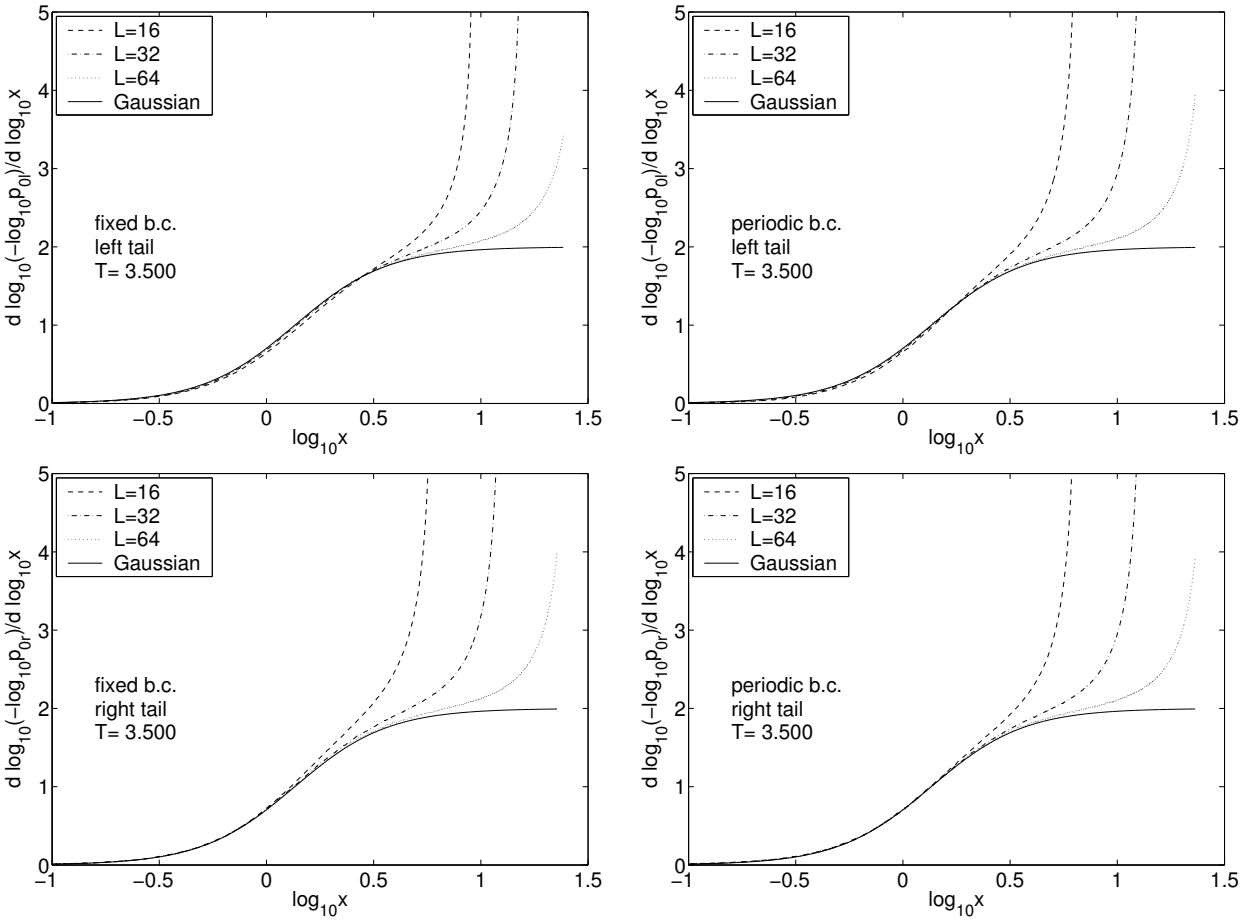

FIGURE 5. Tail analysis for $T = 3.5$. The solid lines represent the standard normal (Gaussian) distribution given in eq. (24).

[72.1.1.1] In the following we plot the results of our tail analysis for three selected temperatures $T = 1.5$, $T = 2.2691 \approx T_c$ and $T = 3.5$. *[72.1.1.2]* We have chosen these temperatures to demonstrate the degree of convergence with respect to L below T_c, at T_c and above T_c. *[72.1.1.3]* Below and above T_c the central limit theorem predicts Gaussian tails which would correspond to a plateau at 2 in our plots. *[72.1.1.4]* At T_c theory predicts a right tail of the form $x^7 \exp(-x^{16})$ corresponding to a plateau at 16.

[72.1.2.1] In Figures 5-7 these are presented for three different temperatures. *[72.1.2.2]* Each of the three figures shows the left tail in the upper row and the right tail in the lower row of the figure. *[72.1.2.3]* Fixed boundary conditions appear in the left column, and periodic boundary conditions in the right column.

[72.1.3.1] All the plots in Figure 5 for the high temperature $T = 3.5$ are similar. *[72.1.3.2]* All tails approach the solid line from the top as L is increased. *[72.1.3.3]* The solid line represents a Gaussian distribution as expected from the central limit theorem. *[72.1.3.4]* However, all the data, even those for $L = 64$, match the Gaussian form over a relatively narrow range in $\log_{10} x$. *[72.1.3.5]* Note that this match still means agreement over many orders of magnitudes in the probability. *[72.1.3.6]* In our analysis the plateau at 2 is beginning to become visible in the data. *[72.1.3.7]* The emergence of the Gaussian tails $\sim \exp(-x^2/2)$ is slow, and system sizes of at least $L \approx 256$ are necessary to clearly show the plateau at 2.

[72.1.4.1] Figure 6 shows the results for the tails of the critical order parameter distribution. *[72.1.4.2]* The curves for the left tails (upper row) for all the three different system sizes nearly collapse. *[72.1.4.3]* Deviations appear only at larger values of the scaling variable x. *[72.1.4.4]* The data collapse makes it difficult to see any systematic approach to the limiting function for infinite systems. *[72.1.4.5]* It should be kept in mind that the scaling function has not reached its form for infinite systems, because the data collapse extends only over a narrow absolute range in the scaling variable x. *[72.1.4.6]* For fixed boundary conditions a plateau seems to develop at around 0.75. *[72.1.4.7]* It would correspond

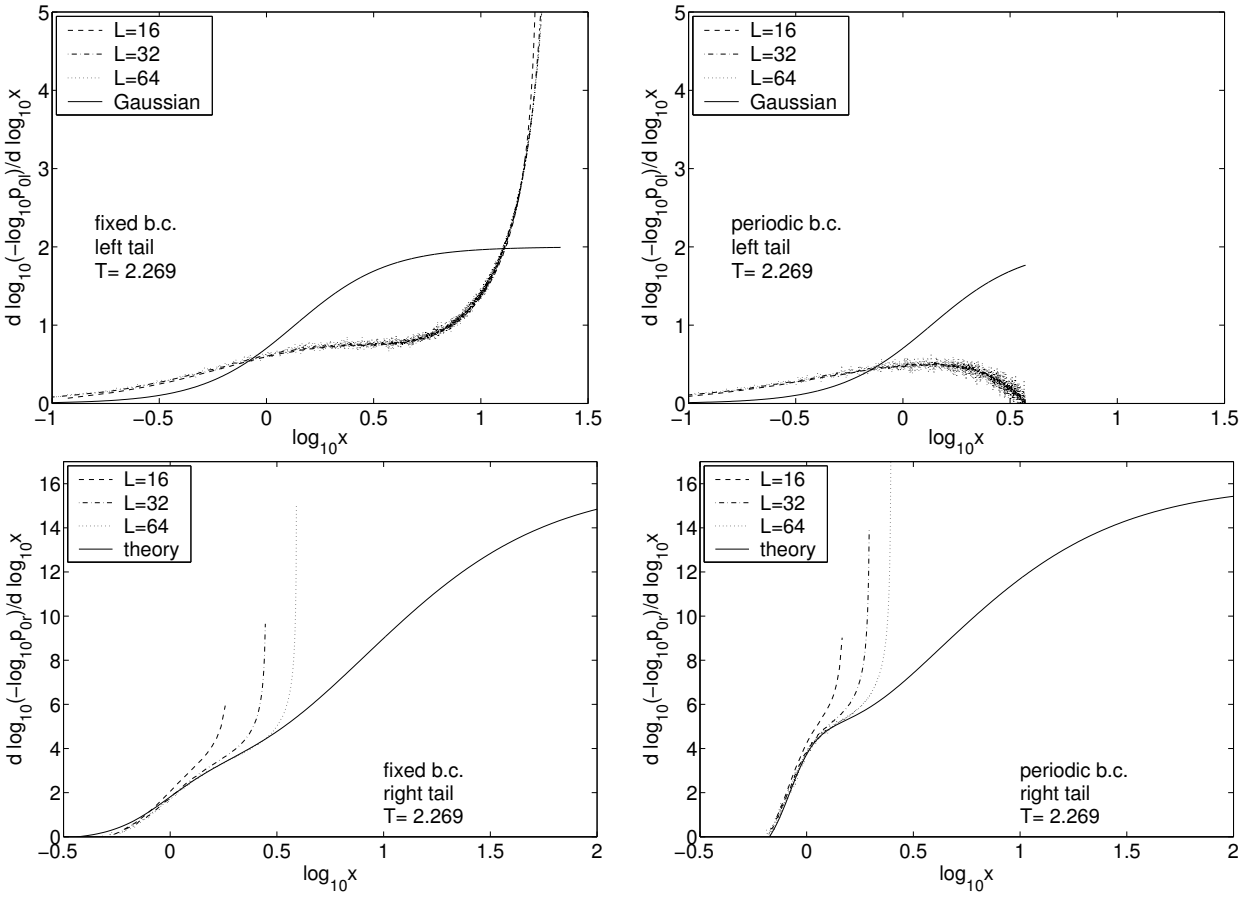

FIGURE 6. Tail analysis for $T = T_c$. The solid lines in the two upper figures represent the standard normal (Gaussian) distribution given in eq. (24). In the lower figures the solid lines are guides to the eye based on fitting the far right tails with $p_0(x) = a((x+c)/b)^7 \exp(-((x+c)/b)^{16})$ where $a = 1.31$, $b = 8.59$, $c = 7.79$ for fixed and $a = 1.45$, $b = 4.59$, $c = 3.69$ for periodic boundary conditions.

to an anomalous stretched exponential tail of the scaling function. *[72.1.4.8]* To the best of our knowledge this has not been observed or predicted up to now.

[72.1.5.1] Next we turn to the right tail of the order parameter distribution at T_c. *[72.1.5.2]* This tail is expected to behave as $\sim x^7 \exp(-x^{16})$ corresponding to a plateau at 16 for large x [4, 3]. *[72.1.5.3]* Our data reveal a shoulder developing with increasing L. *[72.1.5.4]* We have fitted the right tail using this theoretical prediction. *[72.1.5.5]* The fit is shown as a guide to the eye in Figure 6 using eq. (23) with appropriate fit parameters. *[72.1.5.6]* Because of the shift parameter C in eq. (20) the predicted plateau at 16 appears for fully MCS-converged simulations at larger values of L.

[72.1.6.1] Figure 7 for $T = 1.5$ shows some important results. *[72.2.0.2]* First consider the left tails in the upper row. Near the peak (i.e. for small x), the curves approach Gaussian behaviour as one would expect from the central limit theorem [13]. *[72.2.0.3]* However, there is only a relatively narrow regime over which Gaussian behaviour is seen. *[72.2.0.4]* In the intermediate range of x the curves for the left tail show a plateau occuring at 0.5 corresponding to a fat stretched exponential tail $\sim \exp(-\sqrt{x})$. *[72.2.0.5]* In Figure 8 we show the full rescaled order parameter distributions at $T = 1.5$. *[72.2.0.6]* In the upper right hand corner of Figure 8 one sees a narrow Gaussian peak near $x = 0$. *[72.2.0.7]* It is followed by a stretched exponential tail. *[72.2.0.8]* For periodic boundary conditions the stretched exponential tail crosses over into a flat bottom. *[72.2.0.9]* For fixed boundary conditions the same stretched exponential tail is cutoff by a cutoff function. *[72.2.0.10]* The stretched exponential tail represents the well known droplet regime found analytically by Shlosman [29]. *[72.2.0.11]* We found this stretched exponential tail in the distributions for the low temperatures all the way up to the critical temperature. *[72.2.0.12]* Finally in the far tail regime the cutoff function lets the curves diverge to infinity for fixed boundary condi-

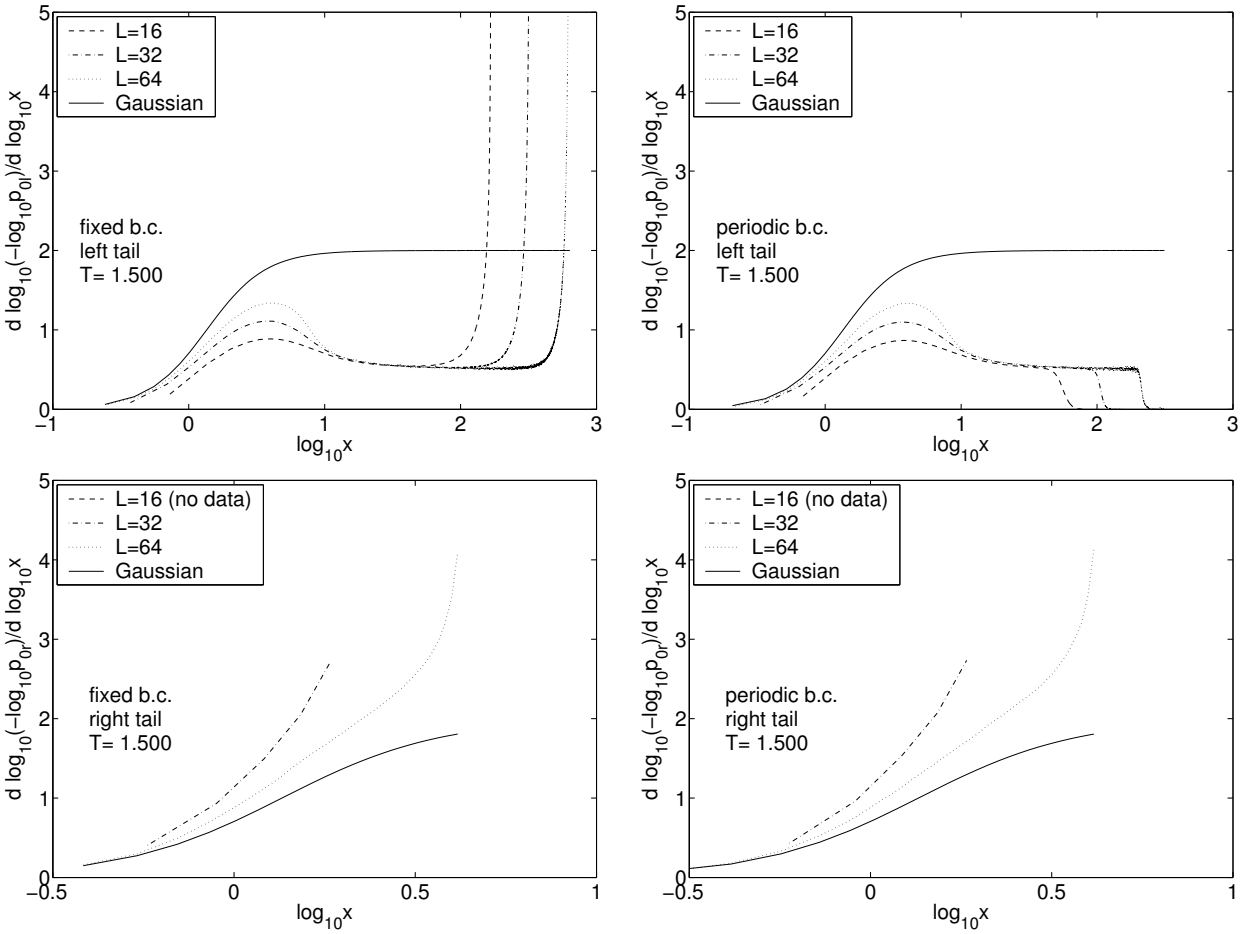

FIGURE 7. Tail analysis for $T = 1.5$. The solid lines represent the standard normal (Gaussian) distribution given in eq. (24).

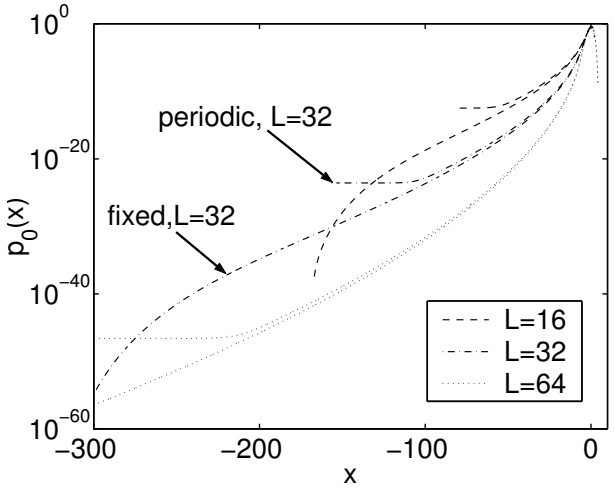

FIGURE 8. Rescaled order parameter distributions $p_0(x)$ for $T = 1.5$ and $L = 16, 32, 64$ for fixed and periodic boundary conditions. (Only right half is shown for periodic boundary conditions).

tions. *[72.2.0.13]* In the case of periodic boundary conditions the order parameter distribution becomes a small constant corresponding to the value zero in our way of plotting the data. *[72.2.0.14]* This is again a well known phenomenon [29], reflecting phase coexistence on finite lattices governed by strip-like spin configurations.

[72.2.1.1] Next we turn to the right tails at $T = 1.5$. *[72.2.1.2]* Because the temperature is very low the magnetization is close to unity. *[72.2.1.3]* Therefore a peak develops only for larger system sizes explaining the absence of data for $L = 16$. *[72.2.1.4]* Even for $L = 32$ only five data points exist to the right of the peak, and hence we can only conclude that the right tails seem to approach Gaussian behaviour with increasing L.

D. **Convergence estimate**

[72.2.2.1] Our results above show clearly that system sizes up to $L = 64$ do not allow to determine the order parameter distribution at criticality. *[72.2.2.2]* Even away from criticality such system sizes are not sufficient

to estimate the true Gaussian behaviour of the tails that has to emergein an infinite system.

[72.2.3.1] It is therefore of interest to estimate the values of L that would suffice to obtain the true order parameter distribution at the critical point. We discuss two *ad hoc* methods for such an estimate.

[72.2.4.1] In the first method we extrapolate the peaks in Figures 2 and 3, and demand that Δ be smaller than some small threshold, e.g. $\Delta < 0.1$. *[72.2.4.2]* In Figures 9 and 10 we show extrapolations of Δ based on power law and logarithmic fits. *[72.2.4.3]* We were unable to fit the data to an exponential fit function.

[72.2.5.1] We emphasize once more that the data points for $L = 128$ are not MCS-converged and hence not fully reliable. *[72.2.5.2]* We also emphasize that the extrapolations are not meant to be accurate. *[72.2.5.3]* Their only purpose is to provide *[page 73, §0]* an order of magnitude estimate for the values of L that we believe are needed to find the true L-converged critical order parameter distribution. *[73.1.0.1]* Extrapolations from both, periodic and fixed boundary conditions, give values larger than $L \approx 10^5$. *[73.1.0.2]* Of course these values increase further if one demands that the threshold value for Δ is smaller than 0.1.

[73.1.1.1] A second method to estimate which values of L are needed for the true L-converged form of the critical order parameter distribution is to demand that the critical data collapse should extend up to values of around 10 in the scaling variable $x = mL^{1/8}$. *[73.1.1.2]* The range over which the data collapse determines the range over which the critical scaling function can be considered to be known. *[73.1.1.3]* From Figure 6 one sees that this range is only of the order $x \approx 1$ in our simulations. *[73.1.1.4]* A range of $x \approx 10$ might still be too small if one wants to decide whether or not the distribution develops algebraic tails. *[73.1.1.5]* Using a value of $x \approx 10$ as a lower bound and remembering that $|m| \leq 1$ one finds $L \approx 10^8$. *[73.2.0.6]* Again this value is very high and in qualitative agreement with the high values found from the first extrapolation method.

[73.2.1.1] Although we have analysed only periodic and fixed boundary conditions here, some other boundary condition could be more relevant for such a study. *[73.2.1.2]* At criticality, a fully converged distribution must correspond to a value of $\Delta(T_c, L)$ close to zero. *[73.2.1.3]* We find $\Delta(T_c, 64)$ for periodic boundary condition to be smaller than $\Delta(T_c, 64)$ for fixed boundary condition. *[73.2.1.4]* So, perhaps, some other boundary condition may give the true critical order parameter distribution at a lower value of L than the extrapolated system sizes anticipated for these boundary conditions from the above analysis.

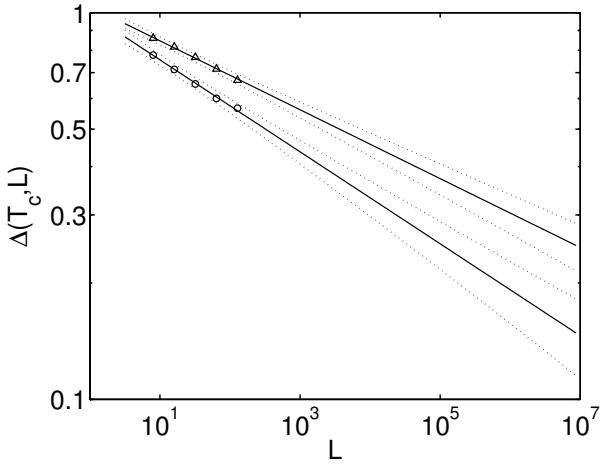

FIGURE 9. Fit and extrapolation using power-law fit function $\Delta = aL^b$ for fixed (triangles) and periodic (circles) boundary conditions. The fit parameters are $a = 1.039(35)$ and $b = -0.0891(98)$ for fixed boundary conditions and $a = 0.993(47)$ and $b = -0.118(15)$ for periodic boundary conditions. The errors in brackets represent 95% confidence intervals. They are represented in the figure as dotted lines following the fit (solid line).

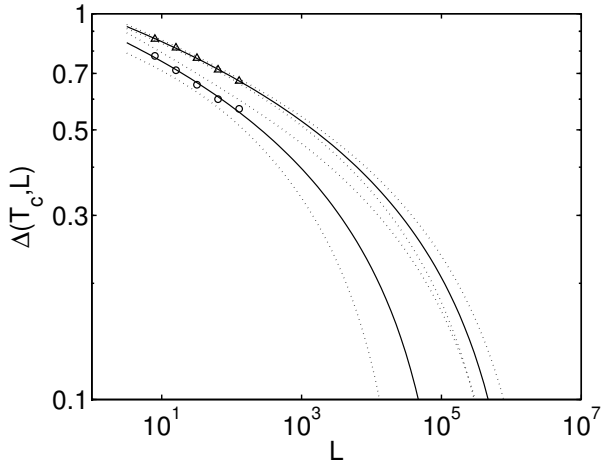

FIGURE 10. Fit and extrapolation using a logarithmic fit function $\Delta = a\log(1/L) + b$ for fixed (triangles) and periodic (circles) boundary conditions. The fit parameters are $a = 0.0694(34)$, $b = 1.006(12)$ for fixed boundary conditions and $a = 0.077(15)$, $b = 0.930(55)$ for periodic boundary conditions. The errors in brackets represent 95% confidence intervals. They are represented in the figure as dotted lines following the fit (solid line).

V. Conclusion

[73.2.2.1] Our main conclusion in this paper is that the universal scaling function for the order parameter distribution at the critical point cannot be considered to be known from numerical simulations at present. *[73.2.2.2]* Our extrapolations indicate that current methods to estimate this quantity require system sizes that are beyond present day numerical resources even for the two-dimensional Ising model. *[73.2.2.3]* Our differential analysis shows that system sizes of at least $L \gtrsim 10^5$ are needed to reach the asymptotic regime at criticality. *[73.2.2.4]* All our findings indicate that convergence with system size is generally very slow. *[73.2.2.5]* For fixed boundary conditions this includes even the convergence of Δ to zero far above the critical point.

References

[1] J. Cardy(ed.), *Finite-Size Scaling* (North-Holland, Amsterdam, 1988).
[2] V. Privman(ed.), *Finite-Size Scaling and Numerical Simulation of Statistical Systems* (World Scientific, Singapore, 1990).
[3] R. Hilfer and N.B.Wilding, J. Phys. A: Math. Gen. **28**, L281 (1995).
[4] G. Smith and A. Bruce, J. Phys. A: Math. Gen. **28**, 6623 (1995).
[5] J. Caillol, D. Levesque, and J. Weis, Phys.Rev.Lett. **77**, 4039 (1996).
[6] J. Kim, A. Souza, and D. Landau, Phys.Rev.E **54**, 2291 (1996).
[7] X. Chen, V. Dohm, and A. Talapov, Physica A **232**, 375 (1996).
[8] A. Bruce, Phys.Rev.E **55**, 2315 (1997).
[9] D. Stauffer, Int. J. Mod. Phys. C **9**, 625 (1998).
[10] M.Tsypin and H. Blöte, Phys.Rev.E **62**, 73 (2000).
[11] H. Blöte, J. Heringa, and M.Tsypin, Phys.Rev.E **62**, 77 (2000).
[12] S. Queiroz and R. Stinchcombe, Phys.Rev.E **64**, 36117 (2001).
[13] K. Binder, Z.Phys.B **43**, 119 (1981).
[14] A. Bruce, J. Phys. C **14**, 3667 (1981).
[15] E. Brezin and J. Zinn-Justin, Nucl.Phys.B **257**, 867 (1985).
[16] A. Esser, V. Dohm, M. Hermes, and J. Wang, Z.Phys.B **97**, 205 (1995).
[17] T. Burkhardt and B. Derrida, Phys. Rev. B **32**, 7273 (1985).
[18] R. Hilfer, Physica Scripta **44**, 321 (1991).
[19] R. Hilfer, Phys. Rev. Lett. **68**, 190 (1992).
[20] R. Hilfer, Mod. Phys. Lett. B **6**, 773 (1992).
[21] R. Hilfer, Int.J.Mod.Phys.B **7**, 4371 (1993).
[22] R. Hilfer, Phys. Rev. E **48**, 2466 (1993).
[23] R. Hilfer, Z. Physik B **96**, 63 (1994).
[24] K. Binder, in *Finite Size Scaling and Numerical Simulation of Statistical Systems*, edited by V. Privman (World Scientific, Singapore, 1990), p. 173.
[25] B. McCoy and T. Wu, *The Two Dimensional Ising Model* (Harvard University Press, Cambridge, 1972).
[26] B. Berg and T. Neuhaus, Phys.Rev.Lett. **68**, 9 (1992).
[27] W. Janke, Physica A **254**, 164 (1998).
[28] N. Ito, Prog. Theor. Phys. **83**, 682 (1990).
[29] S. B. Shlosman, Commun.Math.Phys. **125**, 81 (1989).

(R. Hilfer, B. Biswal) ICA-1, Universität Stuttgart, Pfaffenwaldring 27, 70569 Stuttgart, Germany

(R. Hilfer) Institut für Physik, Universität Mainz, 55099 Mainz, Germany

(B. Biswal) Department of Physics, Sri Venkateswara College, University of Delhi, New Delhi - 110 021, India

(H.G. Mattutis) Tokyo University of Electro-communications, Dept. of Mechanical and Control Engineering, Chofu, Tokyo 182-8585, Japan

(W. Janke) Institut für Theoretische Physik, Universität Leipzig, Augustusplatz 10/11, D-04109 Leipzig, Germany